INFLUENCE OF TURBULENCE CLOSURE ON FREE-SURFACE FLOW MODELLING WITH SPH

Violeau Damien, Issa Réza

EDF R&D / LNHE, 6 quai Watier, 78400 Chatou, France
Phone: +33 1 30 87 78 31; fax: +33 1 30 87 80 86; e-mail: damien.violeau@edf.fr

ABSTRACT

The SPH method is widely used to model complex free-surface flows. The question of viscous models has been examined by many authors but the necessity and choice of an appropriate turbulent model are still not clear. Five turbulent closure models are tested here, from the simplest constant eddy viscosity model to a rather sophisticated non-linear eddy viscosity approach. The considered test case, a gate opening in a tank (for which measurements are available), showed that turbulence modelling is necessary to model the shape of the free surface with accuracy. However, a one-equation model seems to be sufficient to obtain satisfactory results. It is not clear whether the remaining (small) differences between the simulations and the experimental flow are due to physical modelling or numerical features.

Keywords: SPH, free-surface flow, turbulence, RANS models

1 INTRODUCTION

Due to its Lagrangian form, SPH (Smoothed Particle Hydrodynamics) is known as an appropriate method for modelling complex free-surface flows. Many authors still consider that a constant viscosity or even an artificial (numerical) viscous model are enough for SPH flow modelling. On the other hand, specific developments have concerned turbulent closure models applied to SPH in the past few years (see *e.g.* Shao and Gotoh, 2004). Violeau and Issa (2007) have also developed several models and carried out extensive validations including near-wall and unsteady free-surface flows. However, the necessity of using turbulent closure to model free-surface flows is not obvious. For instance, it is commonly accepted that water wave propagation can be considered as the typical example of an inviscid flow; this is the consequence of the fact that this type of flow is mainly governed by gravity forces and inertia. On the contrary, wave breaking involves high deformation and consequently produces significant turbulent stresses which can influence the velocity distribution and thus the shape of the free surface, the efforts induced on a coastal structure, etc. In summary, an important question is how important is turbulence in free-surface driven flow modelling. More precisely, one may ask when a turbulent closure is required and what type of turbulence model is more appropriate to model complex free-surface flows. In this paper we investigate the influence of turbulence closure in the case of a rapid gate opening in a tank. Experiments are compared with simulations achieved by the SPH method using different turbulent models, all of them based on Reynolds-averaged Navier-Stokes (RANS) equations closed with various eddy viscosity models.

2 TURBULENT SPH MODELS

We first remind the main SPH definitions and features (section 2.1). Then the five turbulent models used here are briefly described (section 2.2).

2.1 SPH BACKGROUND

SPH models a flow by a set of 'particles' (in reality bulk fluid volumes, denoted by labels a or b). We use the traditional 2D SPH formalism in which each particle a, with position $\mathbf{r}_a$, has a constant mass m_a and carries a density ρ_a, a pressure p_a and a velocity vector $\mathbf{u}_a$, a dynamic (respectively kinematic) viscosity μ_a (respectively $\nu_a = \mu_a / \rho_a$), and more generally different physical quantities. For the purpose of statistical turbulent flow modelling, all physical variables are Reynolds-averaged, which is herein denoted by an overbar, and particles also carry turbulent eddy viscosity tensors $\boldsymbol{\mu}_{T,a}$ and $\boldsymbol{\nu}_{T,a}$. With these assumptions, SPH forms of Reynolds-averaged continuity and momentum equations can be written as

$$\begin{aligned} \frac{d\rho_a}{dt} &= \sum_b m_b \bar{\mathbf{u}}_{ab} \cdot \nabla_a w_{ab} \\ \frac{d\bar{\mathbf{u}}_a}{dt} &= -\sum_b m_b \left(\frac{\bar{p}_a}{\rho_a^2} + \frac{\bar{p}_b}{\rho_b^2} - \frac{\boldsymbol{\mu}_{e,a} + \boldsymbol{\mu}_{e,b}}{\rho_a \rho_b} \frac{\bar{\mathbf{u}}_{ab}}{r_{ab}^2} \mathbf{r}_{ab} \cdot \right) \nabla_a w_{ab} + \mathbf{g} \end{aligned} \tag{1}$$

where $\mathbf{g}$ is the acceleration of gravity, $\mathbf{r}_{ab} = \mathbf{r}_a - \mathbf{r}_b$, $\bar{\mathbf{u}}_{ab} = \bar{\mathbf{u}}_a - \bar{\mathbf{u}}_b$ and $\boldsymbol{\mu}_{e,a} = \mu_a \mathbf{I} + \boldsymbol{\mu}_{T,a}$, where $\mathbf{I}$ is the identity tensor. $\nabla_a w_{ab}$ denotes the gradient of a kernel function $w_h(r_{ab})$ with respect to the co-ordinates of particle a, while r_{ab} is the distance between particles a and b. In the following, we use the 4th-order spline kernel (see *e.g.* Violeau and Issa, 2007). Eqs. (1) are both integrated in time through an explicit Euler scheme. In the momentum equation, eddy viscosity tensors $\boldsymbol{\mu}_{T,a}$ model the effect of turbulent eddies on the mean (averaged) flow; they can be estimated from various models, summarized in the next section.

The pressure is estimated from the following state equation based on a numerical speed of sound c_0 (Monaghan, 1994):

$$\bar{p}_a = \frac{\rho_0 c_0^2}{\gamma} \left[\left(\frac{\rho_a}{\rho_0} \right)^\gamma - 1 \right] \tag{2}$$

This equation models a weakly compressible flow, the speed of sound being fixed as ten times the maximum flow velocity, to ensure relative variations less than 1%.

2.2 EDDY VISCOSITY MODELS

We consider here five closure models for estimating the eddy viscosity tensor, all presented by the authors (Violeau and Issa, 2007):

- A constant eddy viscosity model;
- A mixing length model;
- A one-equation model;
- A two-equation model;
- A non-linear eddy viscosity model.

The first four models consist of setting the eddy viscosity tensor as being isotropic, *i.e.*

$$\boldsymbol{\mu}_{T,a} = \mu_{T,a} \mathbf{I} \tag{3}$$

where the scalar eddy viscosity $\mu_{T,a}$ is defined by various closure equations. The constant eddy viscosity model consists of setting $\mu_{T,a}$ as a constant in time and space (*i.e.* constant for all particles). It is thus similar to a laminar model with a significantly higher value of the viscosity. In general it is recommended to set its value from tests carried out with one of the

other models, more appropriate for turbulence modelling. The second model is based on a mixing length $L_{m,a}$, representing the characteristic lengthscale of eddy diffusity, here chosen as equal to the initial particle distance (which can be considered as the mean particle size). Then the scalar eddy viscosity is defined from the well-known Smagorinski formula:

$$\begin{aligned} \mu_{T,a} &= L_{m,a}^2 S_a \\ S_a &= \sqrt{2\mathbf{S}_a : \mathbf{S}_a} \end{aligned} \tag{4}$$

where $\mathbf{S}_a$ is the mean rate-of-strain tensor, defined as the symmetric part of the mean velocity gradient tensor. Their components are calculated from the following SPH interpolation:

$$\mathbf{S}_a = -\frac{1}{\rho_a} \sum_b m_b \bar{\mathbf{u}}_{ab} \otimes \nabla_a w_{ab} \tag{5}$$

The mixing length model is based on a turbulence in equilibrium and thus cannot correctly represent rapidly changing phenomena. To cure this, the third and fourth models used here are based on the assumption that the scalar eddy viscosity obeys the following traditional dimensional form

$$\nu_{T,a} = C_\mu \frac{k_a^2}{\varepsilon_a} \tag{6}$$

with $C_\mu = 0.09$. The turbulent kinetic energy k_a attached to particle a is then estimated from the following governing equation:

$$\frac{dk_a}{dt} = P_a - \varepsilon_a + \sum_b m_b \frac{\mu_{k,a} + \mu_{k,b}}{\rho_a \rho_b} \frac{k_{ab}}{r_{ab}^2} \mathbf{r}_{ab} \cdot \nabla_a w_{ab} \tag{7}$$

with $\mu_{k,a} = \mu_a + \mu_{T,a} / \sigma_k$, $\sigma_k = 1.0$, $k_{ab} = k_a - k_b$ and

$$P_a = \min\left(\sqrt{C_\mu}, C_\mu S_a \frac{k_a}{\varepsilon_a} \right) k_a S_a \tag{8}$$

is the production rate. Finally, the dissipation rate ε_a can be directly estimated from the following constitutive equation:

$$\varepsilon_a = C_\mu^{3/4} \frac{k_a^{3/2}}{L_{m,a}} \tag{9}$$

In this case, we have a one-equation model (the third model considered here); however it still requires the definition of an *ad hoc* mixing length. On the contrary, the two-equation model (widely referred to as k–ε) doesn't need the knowledge of such a quantity, and consists of specifying the dissipation from a behaviour equation similar to (6):

$$\frac{d\varepsilon_a}{dt} = \frac{\varepsilon_a}{k_a} \left(C_{\varepsilon,1} P_a - C_{\varepsilon,2} \varepsilon_a \right) + \sum_b m_b \frac{\mu_{\varepsilon,a} + \mu_{\varepsilon,b}}{\rho_a \rho_b} \frac{\varepsilon_{ab}}{r_{ab}^2} \mathbf{r}_{ab} \cdot \nabla_a w_{ab} \tag{10}$$

with $\mu_{\varepsilon,a} = \mu_a + \mu_{T,a} / \sigma_\varepsilon$, $\varepsilon_{ab} = \varepsilon_a - \varepsilon_b$, $\sigma_\varepsilon = 1.3$, $C_{\varepsilon,1} = 1.44$ and $C_{\varepsilon,2} = 1.92$ (Launder and Spalding, 1972). Lastly, the fifth model (referred to as non-linear eddy viscosity model and valid in two dimensions only in the form presented here) is no longer isotropic. In this case the eddy viscosity tensor is defined by

$$\boldsymbol{\mu}_{T,a} = \mu_{T,a}\left(\mathbf{I} - C_{2,a}\Omega_a^*\boldsymbol{\omega}\right) \tag{11}$$

with

$$\Omega_a = \sqrt{2\boldsymbol{\Omega}_a : \boldsymbol{\Omega}_a} \qquad \boldsymbol{\omega} = \begin{pmatrix} 0 & 1 \\ -1 & 0 \end{pmatrix}$$
$$\Omega_a^* = \frac{k_a}{\varepsilon_a}\Omega_a \tag{12}$$

$\boldsymbol{\Omega}_a$ being the vorticity tensor (*i.e.* the antisymmetric part of the velocity gradient tensor). In eq. (11), $\mu_{T,a}$ is defined from the k–ε equations (7) and (10), but with a different definition of C_μ in eq. (6), which now depends on space and time, as well as the coefficient $C_{2,a}$:

$$C_{\mu,a} = \frac{B_3}{2}\frac{P_a^* + B_0}{\left(P_a^* + B_0\right)^2 + \left(B_2\Omega_a^*\right)^2}$$
$$C_{2,a} = \frac{B_2}{P_a^* + B_0} \tag{13}$$

where $P_a^* = P_a / \varepsilon_a$ is the dimensionless production rate, solution to the following algebraic equation:

$$P_a^{*3} + 2B_0P_a^{*2} - \left(\frac{B_3}{2}S_a^{*2} - B_2^2\Omega_a^{*2} - B_0^2\right)P_a^* - \frac{B_0B_3}{2}S_a^{*2} = 0 \tag{14}$$

The model constants are $B_0 = 0.8$, $B_2 = 4 / 9$ and $B_3 = 8 / 15$. The advantage of this model is to take account of non-linearity and curvature effects. Besides, eq. (14) provides a better estimation of the production rate than (8).

All these models where previously tested on various test cases and presented in earlier publications, including boundary conditions. The mixing length model is very simple and popular in traditional CFD and gives good results for simple shear flows; it was successfully applied to SPH by Violeau *et al*. (2002). In the case of an open-channel flow the one and two-equation models are also very well known in the framework of standard Eulerian numerical methods and predict better unsteady turbulent flows; they were applied to SPH by Violeau (2004) and Issa and Violeau (2006) with satisfactory results, but could not be tested with accuracy for complex free surfaces. The non-linear eddy viscosity model was first developed by Pope (1975) and Wallin and Johansson (2000), and applied by the authors (Violeau and Issa, 2007) to SPH. It is known to provide much better predictions than the standard k–ε model as soon as high distorsion or rotation effects are involved; however, it is not still clear whether or not this model is of some interest for free-surface flows.

Since the computational time increases (as well as the quality of the predictions) with the complexity of the turbulent models, knowing the specific advantages and drawbacks of each is a key issue for SPH modelling of turbulent free-surface flows. Indeed, SPH is quite computationally demanding and should be equipped with the most appropriate turbulent model, *i.e.* the best balance between accuracy and simplicity. The purpose of this paper is to compare the five presented models on a test case for which accurate observations of free-surface shape are available. We try to highlight the capabilities of each model in this particular case.

3 MODELLING GATE OPENING IN A TANK

Section 3.1 describes the geometry and the characteristics of the case tested in the context of this study; the results are presented and discussed in section 3.2.

3.1 CASE DESCRIPTION

The case is described in Janosi *et al*. (2004) and consists of a 1.18 m long tank initially filled with a water layer of 1.8 cm at rest. A gate contains a water column of length 38 cm and depth 15 cm (figure 1) and opens at time $t = 0$ to let the water collapse into the tank. This flow is referenced as a SPHERIC benchmark test case (see http://cfd.me.umist.ac.uk/sph/) and presents accurate observations of the free surface at different times (see figures 2 to 4). No PIV velocity measurements were given, but one can assume that the distribution of velocities should be in good accordance with experiments to match the free surface, due to its complexity and mobility.

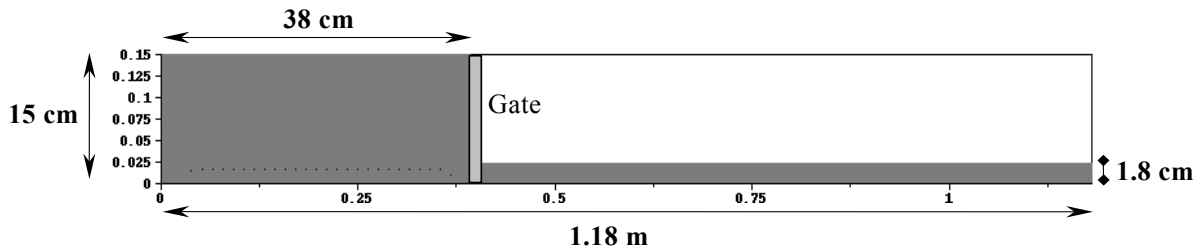

Figure 1 – Geometry of the test case (Janosi *et al.*, 2004).

We chose an initial particle spacing of 1 mm. The walls and the gate are made with "solid" and fictitious particles (see Violeau and Issa, 2007); the total number of particles approaches 80,000. The maximum velocity in the flow was estimated (and checked) to be 2.4 m/s; hence the numerical speed of sound (see section 2.1) was set to 24 m/s.

Results were output every 0.062 s to match experimental measurement times. Experimental results concern the shape of the free surface. One may highlight the fact that a small gap in time (about 43 ms) exists between the experiments and the computed results; for example the first presented graph (figure 2) was numerically obtained at $t = 0.176$ s (instead of $t = 0.219$ s, as indicated on the experimental picture). A first use of the k–ε model showed that the scalar kinematic eddy viscosity $\nu_{T,a} = \mu_{T,a} / \rho_a$ is strongly variable in space. However, its values in the area of interest (*i.e.* breaking) are of the order of magnitude of $3.0\ 10^{-5}\ \mathrm{m^2 s^{-1}}$; this value has been chosen to prescribe $\mu_{T,a}$ in the constant eddy viscosity model.

3.2 RESULTS AND COMPARISON OF TURBULENT MODELS

The results are presented on figures 2, 3 and 4. Figure 2 shows that at $t = 0.219$ s the different models give very similar results, and a satisfactory agreement with experiments is obtained. At this stage, the flow is mainly driven by gravity and inertia, thus the turbulent closure is not important. However, at $t = 0.343$ s the first two models (constant viscosity and mixing length) predict too early the breaking, while the models based on governing equations for k give much better predictions. This may be due to an underestimation of μ_T for all turbulent models based on an turbulent equilibrium assumption (zero-equation models); the time-dependency of turbulent kinetic energy is thus correctly reproduced by eq. (7) at this stage of the flow.

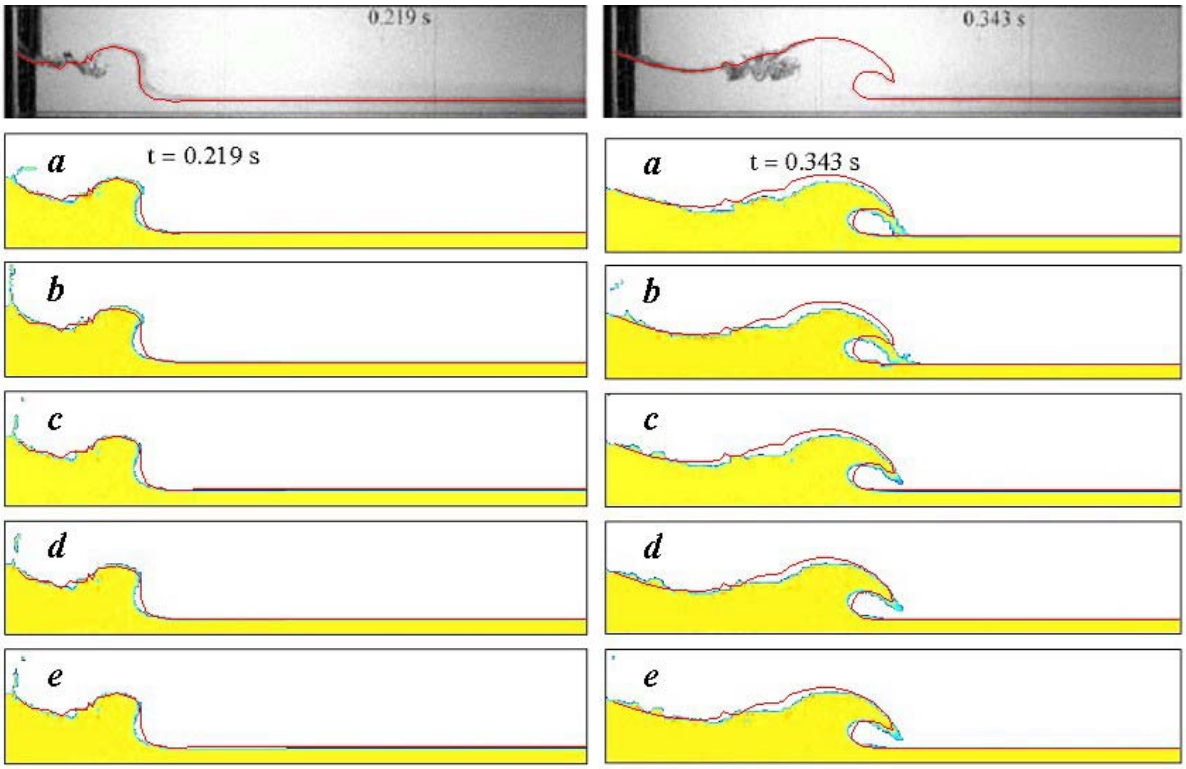

Figure 2 – Comparison of different SPH turbulent closure models with the experiment by Janosi *et al.* (2004) at two different stages (left and right). (a): constant eddy viscosity; (b): mixing length; (c): one-equation; (d): k–ε; (e): non-linear eddy viscosity. The solid lines mimic the experimental free surface.

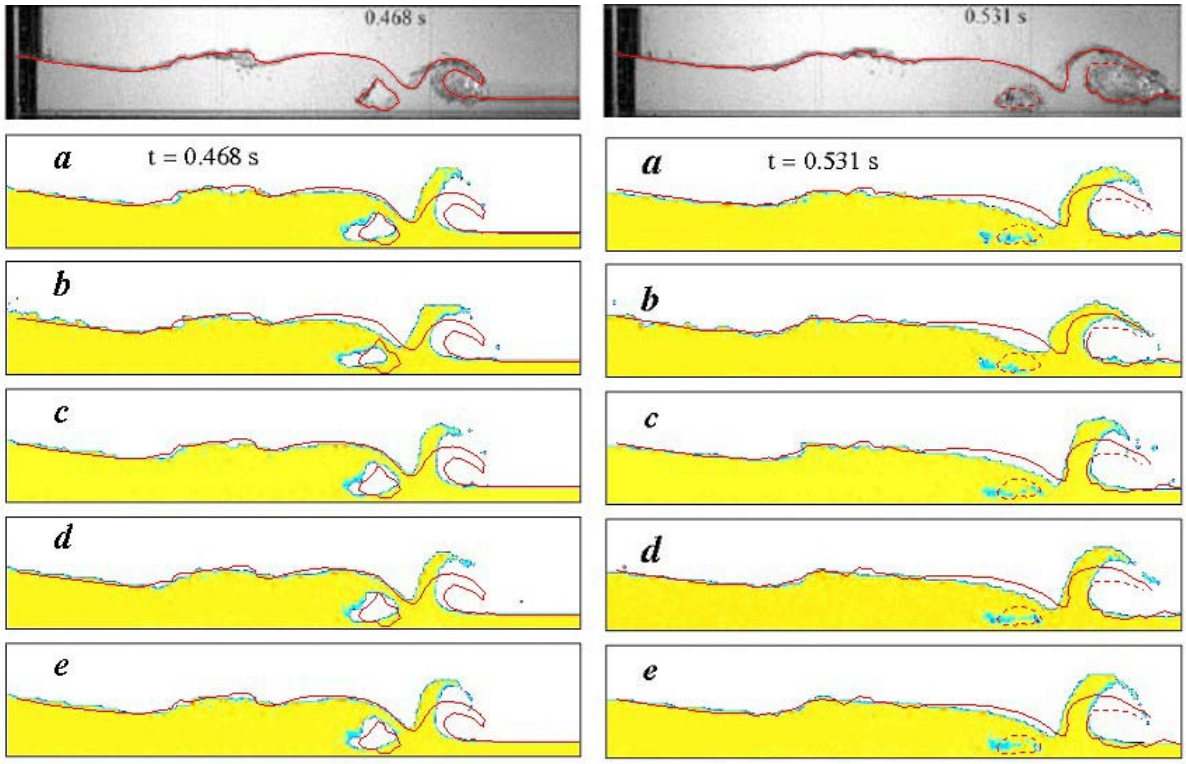

Figure 3 – Same code as figure 2, at later stages.

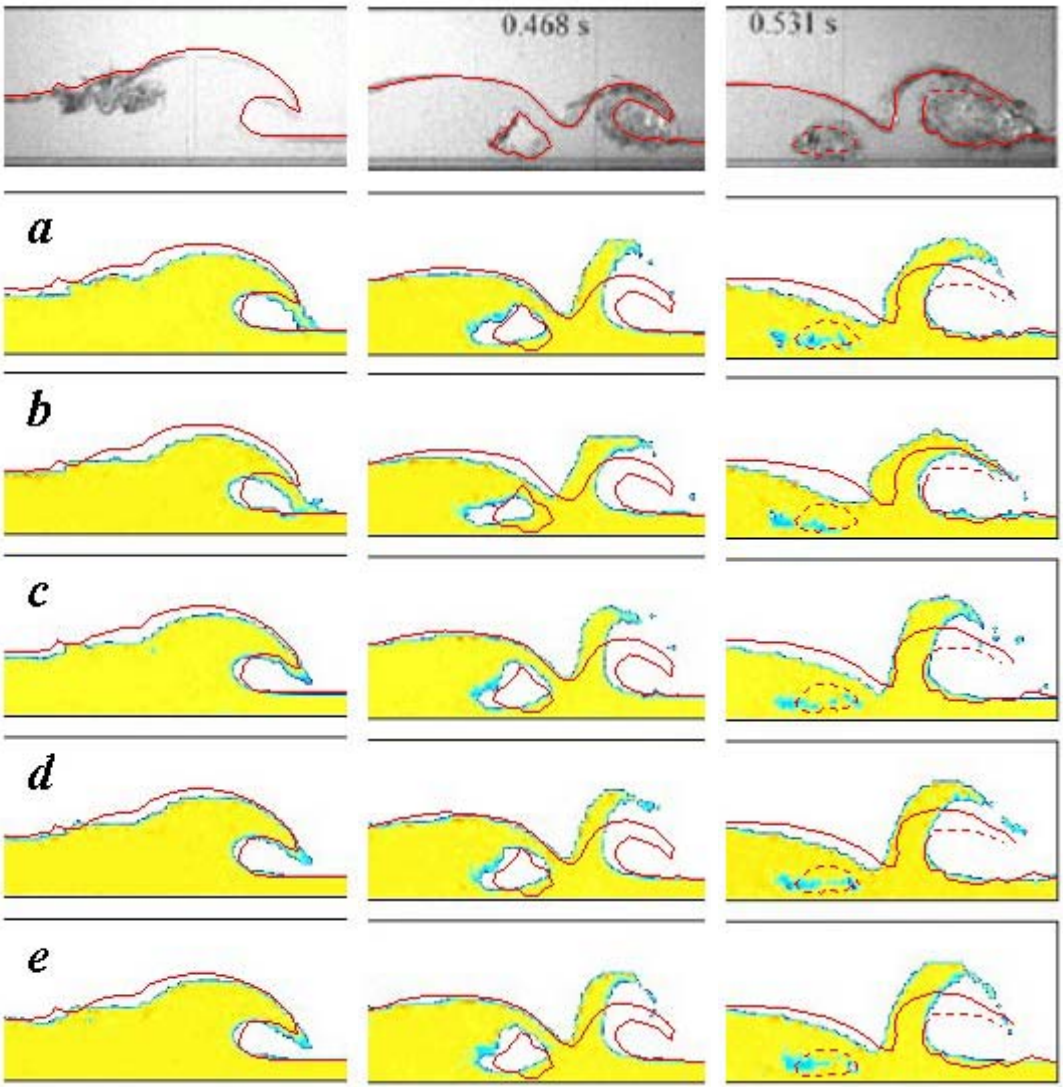

Figure 4 – Zoom on the flow at times t = 0.343 s (left), t = 0.468 s (center) and t = 0.531 s (right). Same code as figure 2.

Figure 3 shows that, surprisingly, the constant viscosity model better predicts the free surface than the mixing length model does at t = 0.468 s, and that the latest significantly underestimates the surface level upstream the breaking. These considerations, confirmed by the zoom presented in figure 4, show that when the breaking occurs, the rate-of-strain S is too strong, and the turbulent timescales too small to consider that the mixing length assumption remains valid. Besides, the shape and size of the void resulting from wave breaking is not correctly reproduced by the first two models. Contrary to this, the other models are more accurate and give similar results to each other, except regarding the shape of the splash-up. Similar observations can be made at time t = 0.531 s. However, the shape of the splash-up is better predicted by the mixing length model, and the water level upstream the splash-up is slightly improved by the non-linear eddy viscosity model (see also figure 4). This analysis tends to prove that eddy viscous forces (*i.e.* Reynolds stresses) become important during and immediately after the breaking stage, due to large and rapidly changing rate-of-strain. To confirm this assumption, one may define an order of magnitude of the ratio between Reynolds stresses and pressure forces:

$$\eta = \frac{\mu_T S}{\overline{p}} \tag{15}$$

Figure 5 shows the spatial distribution of η predicted by the *k*–ε model at different stages. In the main part of the flow, pressure forces remain 20 times higher than turbulent stresses (η < 1/20); however Reynolds stresses become important when approaching the free surface. As the wave breaking develops, they play a more important role in the dynamics of the flow and eventually become predominant in the splash-up area.

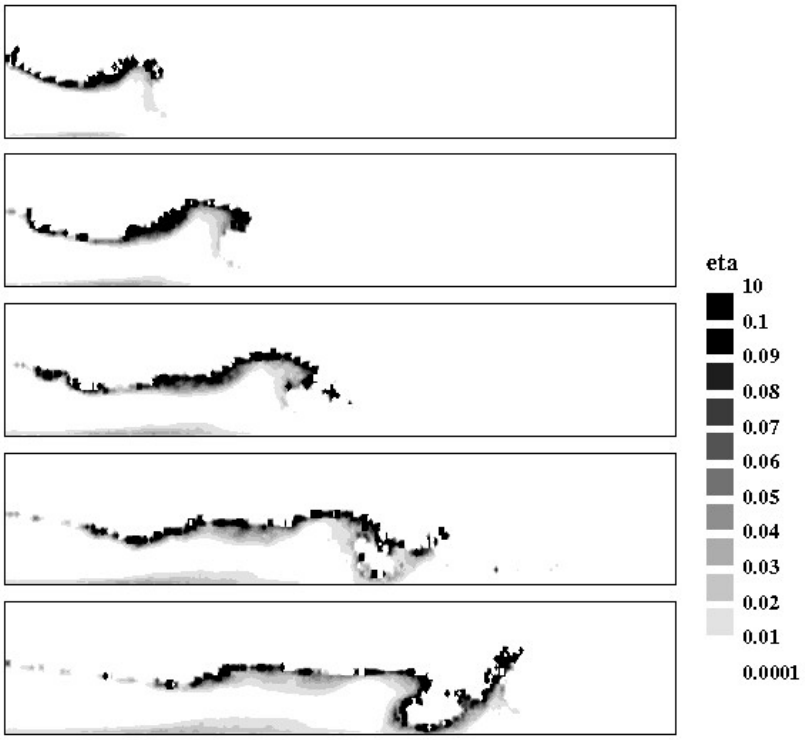

Figure 5 – *k*–ε model. Spatial distribution of η (see eq. (14)) at different stages.

In all the snapshots of figure 3, the height of the splash-up is overestimated, even with the most sophisticated model tested here. It is not clear whether this is due to a lack in physical modelling or to inappropriate numerical features. One may mention that no free-surface condition was prescribed on *k* and ε. However a test with *k* and ε = 0 at the free surface gave very similar results. The spatial discretization or the numerical scheme may also be invoked as partially causing these discrepancies between the experiments and our models. The equation of state (2) is also suspected to be responsible for a poor estimation of pressure, as pointed out by Lee *et al*. (2007), which could affect the quality of the splash-up prediction. It is also clear that simulating this kind of flow with a two-phase model involving water and air, thus allowing the representation of air entrainment during the breaking stage, should increase the quality of the prediction.

Similar conclusions were obtained with an initial water layer of 38 cm (instead of 18), as shown on figure 6. This case were run with three models, namely a constant viscosity (with the same value as previously), a one-equation model and a non-linear eddy viscosity model. Increasing the complexity slightly improves the prediction of breaking and splash-up, but some clear discrepancies remain with measurements.

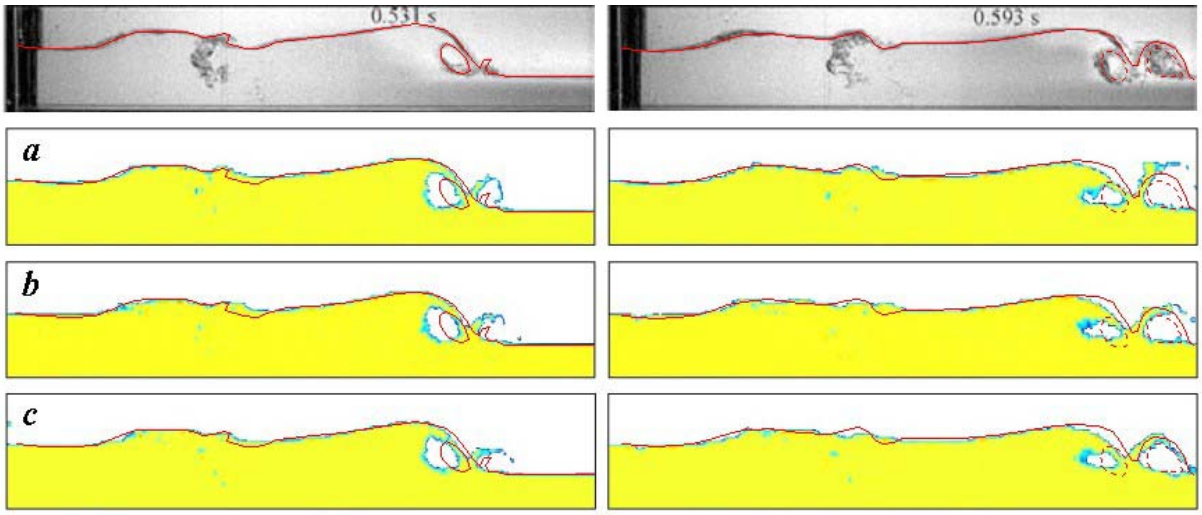

Figure 6 – Comparison of different SPH turbulent closure models with the experiment by Janosi *et al.* (2004) with an initial water layer of 38 cm (instead of 18 cm, as in other figures) at $t = 0.531$ s and $t = 0.593$ (left and right, respectively). (a): constant eddy viscosity; (b): one-equation; (c): non-linear eddy viscosity. The solid lines mimic the experimental free surface.

4 CONCLUSIONS

Five SPH turbulent models were tested on a rather complicated 2D free-surface unsteady flow. It appears that turbulence closure models based on at least one behaviour equation (governing the turbulent kinetic energy) improve the prediction of the shape of the free surface, while the mixing length model is not as good as a simplistic model based on a constant eddy viscosity. However, for the flow examined here, a one equation model seems enough to obtain satisfactory predictions before the splash-up phenomenon; the k–ε and the non-linear eddy viscosity models do not provide any significant improvement in terms of free surface location and shape.

Discrepancies with the experiments are still observed, in particular after the wave breaking (splash-up), for which no clear explanation could be given (physical or numerical). In summary, we recommend, for modelling complicated free-surface flows with SPH, a one-equation model, which seems to be a good balance between accuracy and computational cost.

REFERENCES

Issa, R. and Violeau, D. (2006), *Modelling plunging breaking solitary wave with eddy-viscosity turbulent SPH models*, Comput., Materials and Continua (in press).

Janosi, I.M., Jan, D., Szabo, K.G. and Tel, T. (2004), *Turbulent drag reduction in dam-break flows*, Experiments in Fluids **37**:219-229.

Launder, B.E. and Spalding D.,B., *Mathematical models of turbulence*, Academic Press, London, 1972.

Lee, E.S., Moulinec C., Violeau D., Laurence D. and Stansby P.K. (2007), *Comparisons of weakly compressible and truly incompressible SPH algorithms for 2-D flows*, submitted to the J. Comput. Phys.

Monaghan, J.J. (1994), *Simulating free surface flows with SPH*, J. Comput. Phys. **110**:399–406.

Pope, S.B. (1975), *A more general effective-viscosity hypothesis*, J. Fluid Mech. **2**:331–340.

Shao, S. and Gotoh, H. (2004), *Simulating coupled motion of progressive wave and floatting curtain wall by SPH–LES model*, Coastal Eng. J. **46**:171–202

Violeau, D., Piccon, S. and Chabard, J.P. (2002), *Two attempts of turbulence modelling in Smoothed Particle Hydrodynamics*, Proc. VIIIth Symposium on Flow Modelling and Turbulence Measurements, Advances in Fluid Modelling and Turbulence Measurements, World Scientific, pp. 339–346.

Violeau, D. (2004), *One and two-equations turbulent closures for Smoothed Particle Hydrodynamics*, Proc. VIth Int. Conf. Hydroinformatics, World Scientific, pp. 87–94.

Violeau, D. and Issa, R. (2007), *Numerical modelling of complex turbulent free-surface flows with the SPH method: an overview*, Int. J. Num. Meth. Fluids **53**(2):277-304.

Wallin, N. and Johansson, A.V. (2000), *An explicit algebraic Reynolds stress model for incompressible and compressible turbulent flows*, J. Fluid Mech. **403**:89–132.